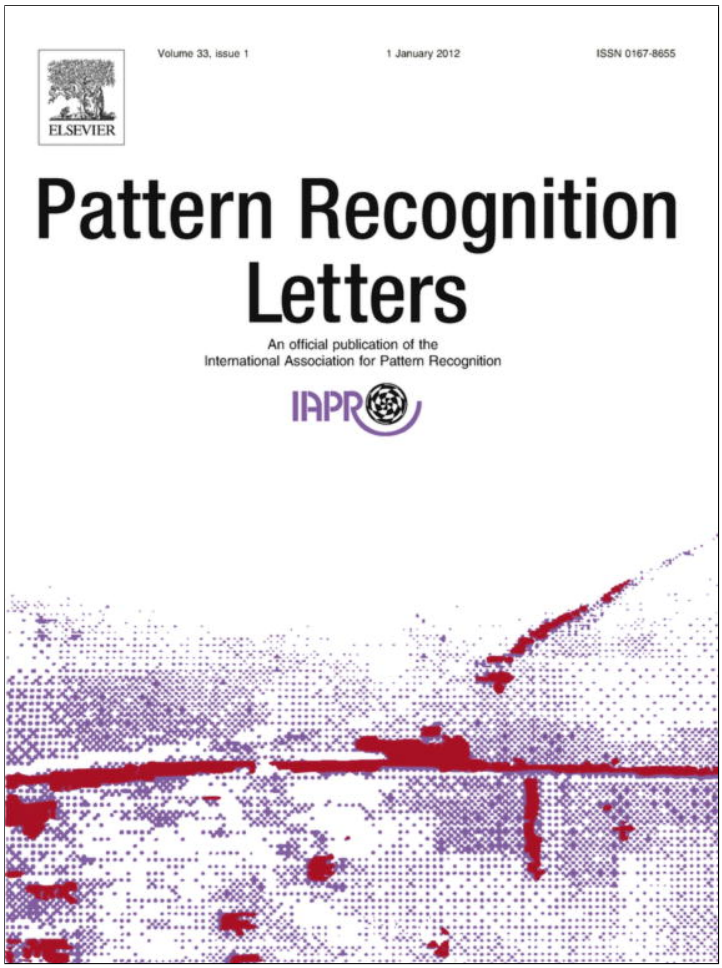

(This is a sample cover image for this issue. The actual cover is not yet available at this time.)

Pattern Recognition Letters 33 (2012) 1180–1187

Contents lists available at SciVerse ScienceDirect

Pattern Recognition Letters

journal homepage: www.elsevier.com/locate/patrec

Harris function based active contour external force for image segmentation

Andrea Kovacs [a,b,*], Tamas Sziranyi [b]

[a] Pazmany Peter Catholic University, H-1083, Prater u. 50/a, Budapest, Hungary
[b] Distributed Events Analysis Group, Computer and Automation Research Institute, H-1111, Kende u. 13-17, Budapest, Hungary

ARTICLE INFO

Article history:
Received 1 June 2011
Available online 10 February 2012
Communicated by A. Koleshnikov

Keywords:
Boundary extraction
Gradient vector flow
Vector field convolution
Harris corner detection

ABSTRACT

Deformable active contour (snake) models are efficient tools for object boundary detection. Existing alterations of the traditional gradient vector flow (GVF) model have reduced sensitivity to noise, parameters and initial location, but high curvatures and noisy, weakly contrasted boundaries cause difficulties for them.

This paper introduces two Harris based parametric snake models, Harris based gradient vector flow (HGVF) and Harris based vector field convolution (HVFC), which use the curvature-sensitive Harris matrix to achieve a balanced, twin-functionality (corner and edge) feature map. To avoid initial location sensitivity, starting contour is defined as the convex hull of the most attractive points of the map. In the experimental part we compared our methods to the traditional external energy-inspired state-of-the-art GVF and VFC; the recently published parametric decoupled active contour (DAC) and the non-parametric Chan–Vese (ACWE) techniques. Results show that our methods outperform the classical approaches, when tested on images with high curvature, noisy boundaries.

1. Introduction

Object boundary detection is an important field of vision research. The active contour (AC) method (or also called as snake) was introduced in (Kass et al., 1988), since then deformable models proved to be efficient tools for robust identification of object contours (Xu and Prince, 1997; Caselles et al., 1997; Brigger et al., 1997; Chan and Vese, 2001; Vasilevskiy and Siddiqi, 2002; Kimmel and Bruckstein, 2003; Bresson et al., 2007; Li and Acton, 2007; Mishra et al., 2011). Snake evolution is controlled by an energy minimizing method based on different energies. Internal energy is responsible for obtaining elastic and rigid curves, while external energy represents the constraints of the image itself and is usually calculated as a function of gradient information over the intensity distribution. This force pushes the snake toward an optimum in the feature space. The traditional snake model has limited utility as the initialization should be close to the real contour of the object. Problems also occur when detecting concave boundaries. To compensate these drawbacks, Gradient vector flow (GVF) snake was introduced in (Xu and Prince, 1997), which defined a new external force as a diffusion of the gradient vectors of a gray-level or binary edge map derived from the image. Although precision improved, GVF snake was still noise, parameter and initialization sensitive.

Since the publication of the original method (Kass et al., 1988), several modification have been developed to compensate the drawbacks of the original algorithm, including parametric (Xu and Prince, 1997; Brigger et al., 1997; Li and Acton, 2007; Mishra et al., 2011) and non-parametric (Caselles et al., 1997; Chan and Vese, 2001; Vasilevskiy and Siddiqi, 2002; Kimmel and Bruckstein, 2003; Bresson et al., 2007) approaches.

Parametric active contours suffer from weaknesses associated with noise, parameter and initialization sensitivity, topology changes and have difficulties when detecting high curvature boundaries. While non-parametric methods do not depend on initialization and detect complex boundaries with sharp corners and topological variations, they fail when detecting objects with broken edges. Additionally their convergence rate is slower and they are more sensitive to noise than the parametric approaches. Application of non-parametric techniques to images of narrow elongated structures, where intensity contrast may be low and reliable region statistics cannot be computed was independently improved by Vasilevskiy and Siddiqi (2002) and Kimmel and Bruckstein (2003); additionally when using shape priors as (Uzunbas et al., 2010), non-parametric methods can also cope with broken edges.

One class of the parametric methods tried to redefine the expression of external energy to improve the accuracy of GVF snake (Chuang and Lie, 2004; Cheng and Foo, 2006; Li and Acton, 2007; Jifeng et al., 2007; Wang et al., 2010; Zhu et al., 2010). While these approaches reduced the sensitivity in some aspects, they still had difficulties when featuring very sharp and noisy corners. These

* Corresponding author at: Pazmany Peter Catholic University, H-1083, Prater u. 50/a, Budapest, Hungary. Tel.: +36 12796106.
E-mail addresses: kovacs.andrea@itk.ppke.hu (A. Kovacs), sziranyi@sztaki.hu (T. Sziranyi).

0167-8655/$ - see front matter © 2012 Elsevier B.V. All rights reserved.
http://dx.doi.org/10.1016/j.patrec.2012.01.018

high curvature, noisy boundary points along with noisy edges are still among the major challenges that existing methods are not able to handle appropriately.

Snake initialization is a challenging task, some representations take shape information into account (Sundaramoorthi and Yezzi, 2007) or extract the focus area to define the region of interest (Kovacs and Sziranyi, 2007), but in case of the detection of randomly shaped objects, the initial outline is usually defined with human interaction. Recently published quasi-automatic method, (Tauber et al., 2010) requires the selection of an arbitrary point in the target region to initialize the curve, but it is not able to segment regions that feature topological changes.

To address the limitation of initialization and curvature sensitivity, this paper proposes two parametric active contour approaches, introduced as the Harris based GVF (HGVF) snake (Kovacs and Sziranyi, 2010) and the Harris based vector field convolution (HVFC) (Kovacs and Sziranyi, 2011), both use a modified function of Harris corner detector (Harris and Stephens, 1988) that benefits from the cornerness feature, therefore, it is suitable for emphasizing both corner points and edges, and attains a balanced feature map. The most attractive points of the map are used to initialize a starting curve around the object, while the modified map is applied to determine a new feature map for the external energy expression.

In the experimental part, we have evaluated the performance of our methods on the Weizmann segmentation database (Alpert et al., 2007) and compared the results to published techniques, including two external energy-inspired parametric algorithms (Xu and Prince, 1997; Li and Acton, 2007); a novel parametric method (Mishra et al., 2011) and a non-parametric, region based (Chan and Vese, 2001) application. According to the evaluation results, our algorithms perform better in detecting high curvature, noisy object boundaries.

2. Active contour model

2.1. Traditional approach

Introduced in (Kass et al., 1988), the goal of active contour or snake (denoted by $\boldsymbol{x}(s) = [x(s), y(s)], s \in [0,1]$) is to minimize the following energy:

$$E = \int_0^1 \frac{1}{2}(\alpha|\boldsymbol{x}'(s)|^2 + \beta|\boldsymbol{x}''(s)|^2) + E_{\text{ext}}(\boldsymbol{x}(s))\mathrm{d}s, \tag{1}$$

where α and β are weighting parameters for the elasticity and rigidity components of the internal energy; $\boldsymbol{x}'(s)$ and $\boldsymbol{x}''(s)$ are the first and second order derivatives with respect to s. The rigidity component is responsible for detecting curvature, setting $\beta = 0$ allows the snake to develop a corner. E_{ext} is the external energy derived from the image, representing the image constraints and giving smaller values at features of interest (like edges and ridges), than at homogeneous regions.

2.2. Gradient vector flow

Xu and Prince (1997) defined gradient vector flow (GVF) as external force for active contour methods. Besides the internal forces, the rigidity and elasticity components, the external force is computed as a diffusion of the gradient vectors of the gray level or binary edge map derived from the image. The increased capture range of the external force field guides the contour toward the boundary, even into concave regions. The novel E_{ext} energy is as follows:

$$E_{ext} = \iint \mu\left(u_x^2 + u_y^2 + v_x^2 + v_y^2\right) + |\nabla f|^2|v - \nabla f|^2 \mathrm{d}x\mathrm{d}y, \tag{2}$$

where the $\boldsymbol{v}(x,y) = (u(x,y), v(x,y))$ is the GVF field that minimizes E_{ext}, μ is a regularization parameter. The f edge map is derived from the image $I(x,y)$. One of the generally used forms is:

$$f(x,y) = |\nabla(G_\sigma(x,y) * I(x,y))|, \tag{3}$$

where G_σ is the Gaussian function with σ standard deviation and ∇ is the gradient operator (Xu and Prince, 1997).

The original f edge map has difficulties when detecting sharp or noisy corners and low contrast boundaries. When heading towards a sharp corner point in the image, the intensity changes largely from only a few directions. This results that these pixels behave similarly like low contrast boundary points: they both have decreased $f(x,y)$ values compared to sharp edges. This effect is shown in Fig. 1, where decreased f values can be seen around the peak of the leaf inside the white rectangle in Fig. 1b. The result of this effect is that the iterative AC method does not detect the peaks accurately (see the third image in the first row of Fig. 4).

2.3. Vector field convolution

Vector field convolution (VFC) was introduced in (Li and Acton, 2007) as external force, addressing the disadvantages of GVF, such as high computational cost, noise sensitivity, parameter sensitivity, and the ambiguous relationship between the capture range and parameters. The VFC field is calculated by convolving a vector field kernel with the edge map generated from the image:

$$\boldsymbol{f}_{\text{VFC}}(x,y) = f(x,y) * \boldsymbol{k}(x,y), \tag{4}$$

where $f(x,y)$ is the original, image based edge map (Eq. (3)) and $\boldsymbol{k}(x,y)$ is the vector field kernel, which is defined as:

$$\boldsymbol{k}(x,y) = m(x,y)\boldsymbol{n}(x,y), \tag{5}$$

where $m(x,y)$ is the magnitude at (x,y) and $\boldsymbol{n}(x,y)$ is the unit vector pointing to the kernel origin: $\boldsymbol{n}(x,y) = \left[-\frac{x}{r}, -\frac{y}{r}\right]$, r denotes the distance from the origin.

The advantage of VFC representation is that a free particle (i.e. a single contour point) placed in the field is able to move to the feature of interest. The $m(x,y)$ magnitude should be chosen as a decreasing positive function of the distance from the origin, such as:

$$m(x,y) = (r + \epsilon)^{-\gamma}, \tag{6}$$

with γ controlling the decrease and ϵ preventing division by zero. As the feature map of VFC (Eq. (4)) is also based on the $f(x,y)$ original edge map, problems of detecting high curvature and noisy, weakly contrasted boundaries still exist (see Fig. 1c and the fifth image in the first row of Fig. 4).

High curvature corners can be found by corner detectors after generating a characteristic function which emphasizes possible corners in the image. Our idea was to apply Harris corner detector as it is reliable and invariant to rotation (Schmid et al., 2000). The original Harris characteristic function is modified to be able to emphasize the high curvature corners and low contrast edges as well by exploiting the curvature information along the boundary and resulting in a balanced feature map.

3. Harris based gradient vector flow (HGVF) and Harris based vector field convolution (HVFC)

Our process first generates the main feature points based on the Harris corner detector, then these points are enveloped to get the initialization of the contour. As a novelty, modification of Harris cornerness function is used instead of edge functions as feature map for generating GVF and VFC snake.

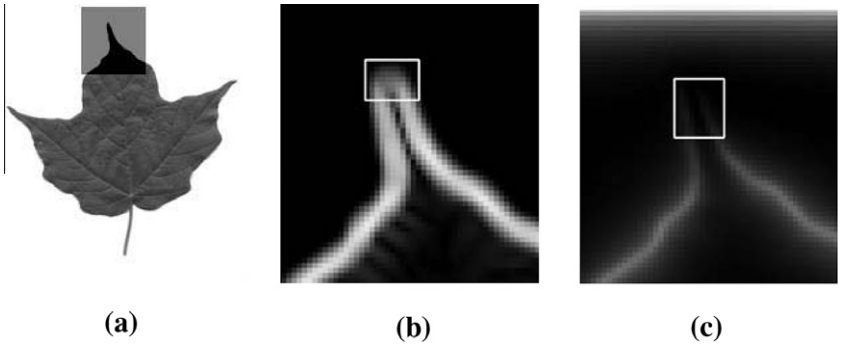

Fig. 1. The original f edge map for high curvature boundary: (a) shows the original image, region of interest is in gray; (b) is the f edge map of the marked area. The white rectangle indicates the decreased f values of the high curvature boundary; (c) is the $\boldsymbol{f}_{\mathrm{VFC}}$ map of the marked area. The white rectangle indicates the decreased $\boldsymbol{f}_{\mathrm{VFC}}$ values of the high curvature boundary.

3.1. Original Harris detector

The Harris detector was introduced in (Harris and Stephens, 1988). The algorithm is based on the principle that at corner points intensity values change largely in multiple directions. According to (Harris and Stephens, 1988), change D for a small shift (x,y) is given by the following Taylor expansion:

$$D(x,y) = Ax^2 + 2Cxy + By^2, \tag{7}$$

which can be rewritten as

$$D(x,y) = (x,y)M(x,y)^T. \tag{8}$$

The method uses the Harris matrix (M):

$$M = \begin{bmatrix} A & C \\ C & B \end{bmatrix}, \tag{9}$$

where $A = \dot{x}^2 \otimes w, B = \dot{y}^2 \otimes w, C = \dot{x}\dot{y} \otimes w$. $\dot{x} = \frac{\partial I}{\partial x}$ and $\dot{y} = \frac{\partial I}{\partial y}$ denote the approximation of the first order derivatives of the I image, $\otimes$ is a convolution operator and w is a Gaussian window.

The curvature behavior around an image point can be well described by the Taylor expansion (Eq. (7)). When D is reformulated by a structure tensor (Eq. (8)) and becomes closely related to the local autocorrelation function, M describes the shape at the image point. The eigenvalues of M will be proportional to the principal curvatures of the local autocorrelation function and form a rotationally invariant description of M (Harris and Stephens, 1988). This feature is beneficial when external forces are calculated to measure salient points of any boundaries, as the principal curvatures describe well the fine details of shapes.

The original Harris corner detector defines the following corner response to select isolated corner pixels:

$$R = \mathrm{Det}(M) - k * \mathrm{Tr}^2(M), \tag{10}$$

where Det and Tr denote the determinant and trace and k is a coefficient, usually around 0.04 (Harris and Stephens, 1988). R is large and positive in corner regions, negative in edge regions and small in the flat regions, therefore, it is inappropriate to emphasize corners and edges equally.

3.2. Harris based feature map

When defining a new feature map for GVF snake, the curvature behavior should be analyzed. Therefore, eigenvalues of M are applied to create a novel characteristic function, emphasizing the curvature around image pixels.

Let λ_1 and λ_2 denote the eigenvalues of M (Eq. (9)). They define separate cases: both of them are large in corner regions, only one of them is large in edge regions and both of them are small in flat regions (Harris and Stephens, 1988). When emphasizing corners and edges, they both have one large component, thus, $max(\lambda_1,\lambda_2)$ function separates the flat and non-flat regions accurately. To produce a steady feature map, the dynamics of the characteristic function should be compressed into a balanced distribution by keeping the necessary strength of the main attractors. The natural logarithmic (log) function satisfies this condition: it has a balanced output for both corner and edge saliency. Consequently, the following R_{logmax} saliency function is proposed in (Kovacs and Sziranyi, 2010) for describing shapes with equally emphasized edge and corner regions:

$$R_{\mathrm{logmax}} = \max(0, \log[\max(\lambda_1, \lambda_2)]). \tag{11}$$

For both edge and corner points $\max(\lambda_1,\lambda_2) \gg 1$. The target set of the R_{logmax} is the positive domain (when it is used as a feature map), thus, the outer max function is responsible for replacing negative values of small λ (points in flat regions) with zeros. Example of the proposed R_{logmax} function can be seen in Fig. 2c.

Now, with a balanced output for both corners and edges, R_{logmax} can be applied efficiently in the feature map:

$$f_{\mathrm{HGVF}}(x,y) = |\nabla(G_\sigma(x,y) * R_{\mathrm{logmax}}(x,y))|. \tag{12}$$

This function will be applied in the Harris based gradient vector flow (HGVF) algorithm. Based on f_{HGVF} the new feature map for Harris based vector field convolution (HVFC) method is as follows:

$$\boldsymbol{f}_{\mathrm{HVFC}} = f_{\mathrm{HGVF}}(x,y) * \boldsymbol{k}(x,y). \tag{13}$$

The comparison of the original and the proposed feature map can be seen in Fig. 2. While the original, intensity based f edge map (Xu and Prince, 1997) losses some low contrast edges on the boundary and fails to emphasize the sharp corners (see Fig. 2b), our proposed f_{HGVF} map (Fig. 2d) is able to feature the real contour more accurately.

3.3. Initial contour

Feature (or saliency) points are chosen as the local maxima of R_{logmax} (Eq. (11)), see Fig. 2e. Since feature points are located on the edges and corners of the object, they can be used to define an initial contour. To avoid the poor definition of smooth transition or multi-directional saddle effects of edges around corners, the surroundings of the saliency points should be taken into account. Therefore, a local area with a 3 pixel radius around the point should be considered as part of the region of interest (ROI), where relevant local structures can be detected. Points representing the outline of the supported area should be added to the Harris feature point set. After this, the initial contour is defined as the convex hull

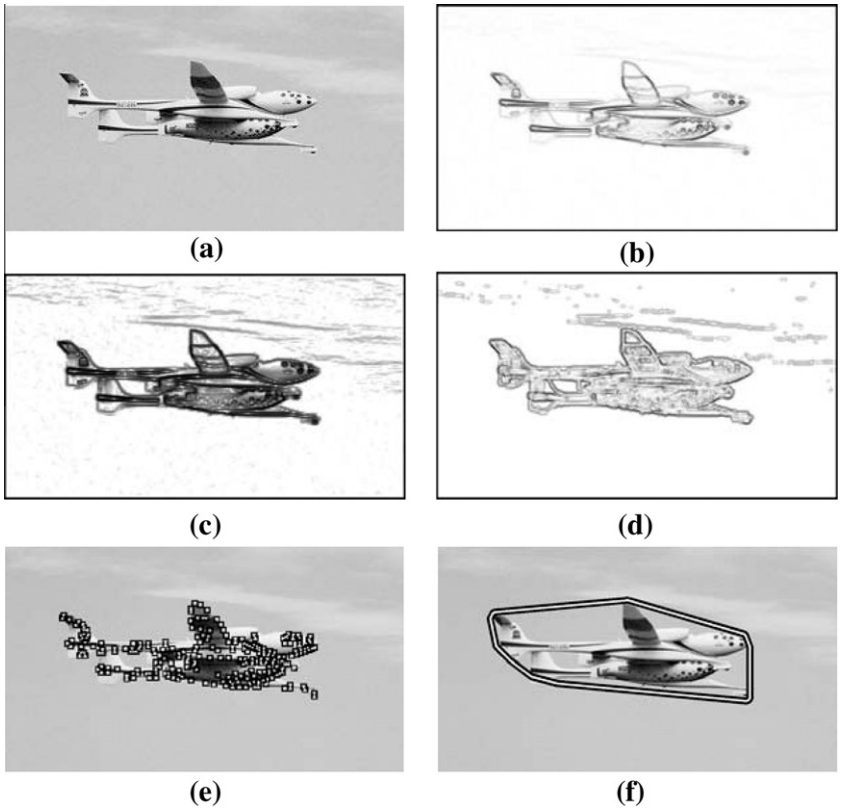

Fig. 2. Effect of R_{logmax} characteristic function: (a) is the original image; (b) is the original, f intensity based map of GVF; (c) is the generated and inverted R_{logmax} characteristic function; (d) is the proposed f_{HGVF} Harris based map for GVF (Eq. (12)); (e) shows the generated salient points as the local maxima of the R_{logmax} function (Fig. 2(c)); (f) is the initial contour based on the convex hull of the corner points.

of the extended set of points denoted by P (see Fig. 2(f)). Convex hull has already been used for initializing active contour (Sirakov, 2006; Zamani and Safabakhsh, 2006), our innovation resides in the extended Harris based contour point set for localizing the object.

The convex hull of P set of points is the smallest convex set that contains the points. It can be characterized as the set of all of the convex combinations of finite subsets of points from P and looks as follows:

$$H_{\text{convex}}(P) = \left\{ \sum_{i=1}^{k} \alpha_i p_i : p_i \in P,\ \alpha_i \in \mathbb{N},\ \alpha_i \geqslant 0, \right.$$
$$\left. \sum_{i=1}^{k} \alpha_i = 1,\ k = 1, 2, \ldots \right\}. \tag{14}$$

A wide range of algorithms is known for constructing the convex hull for a finite point set with various computational complexities. In our implementation we applied the built-in function of MATLAB, which uses the 'Qhull' algorithm (Barber et al., 1996). Let n denote the number of points in P and h the number of points in the hull, then the computational complexity of the calculation of the hull is $O(n \log h)$.

Our algorithms follow the operation of traditional GVF and VFC methods, but proceed from the convex hull of the feature points ($H_{\text{convex}}(P)$) and utilize the new f_{HGVF} and $\boldsymbol{f}_{HVFC}$ maps instead of simple f in the external force component. (See Eq. (2).) Therefore, the behavior of the proposed algorithms is similar to the traditional approaches, including parameter settings. When constructing the novel feature maps, the Gaussian window (see Section 2.2) have to be chosen, determining the smoothness of the map. In our experiments, we used the w Gaussian window, with $\sigma = 0.2$ for images without noise and $\sigma = 1.5$ for all the noisy images. Apart from this parameter, the proposed algorithms uses the parameters of the traditional active contour approaches, thus, the sensitivity to parameter tuning is analyzed in (Xu and Prince, 1997 and Li and Acton, 2007).

4. Experimental results and discussions

In this experimental part we evaluated our proposed methods quantitatively using the Weizmann segmentation evaluation database (Alpert et al., 2007) and qualitatively on specific images, representing various characteristics: objects with weak edges or high curvature boundary parts and noisy images (Fig. 4). The performance of the proposed methods was compared to traditional parametric and non-parametric active contour algorithms. Gradient vector flow (GVF) (Xu and Prince, 1997) and vector field convolution (VFC) (Li and Acton, 2007) were selected to show the improvement of effectiveness due to the introduced feature map. Region based methods can detect high curvature boundaries accurately, therefore, the non-parametric active contour without edges (ACWE) (Chan and Vese, 2001), based on the Chan–Vese model have also been evaluated. Decoupled active contour (DAC) (Mishra et al., 2011) method has recently been introduced and was found to be able to detect regions of high curvatures and converging rapidly, thus, an image from the referenced paper was used for comparing our method to DAC.

For evaluation, we used the published MATLAB source code of the compared algorithms without optimization. Parameter settings for the compared methods were chosen according to the mentioned references.

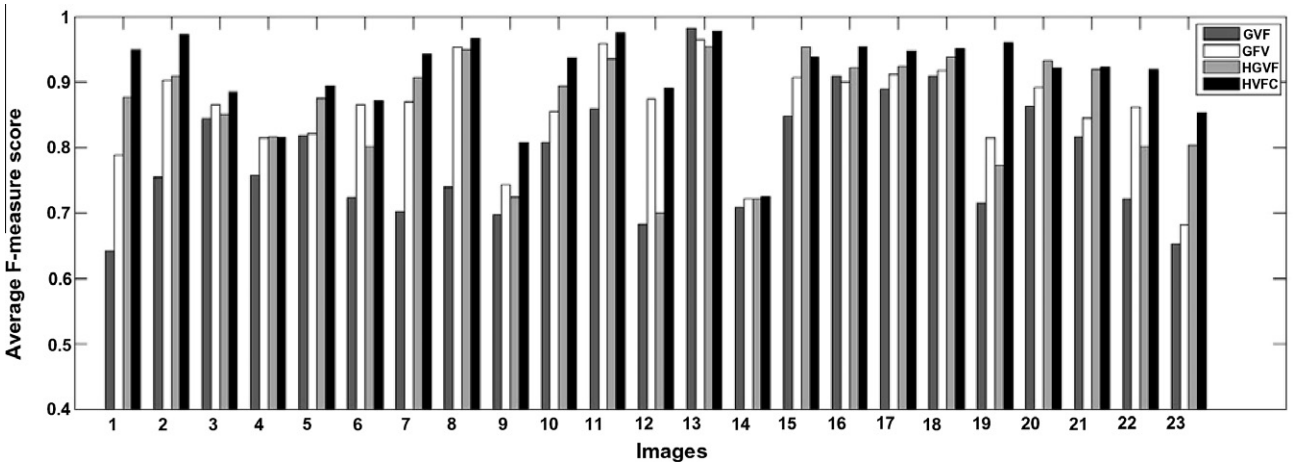

Fig. 3. Detailed evaluation results. Vertical axis shows the achieved average *F*-measure score for each test image separately. Horizontal axis shows the numbered images from the Weizmann database (Alpert et al., 2007) used for the evaluation set. Separate bars indicate the results of different methods: light gray is GVF (Xu and Prince, 1997), white is VFC (Li and Acton, 2007), dark gray is HGVF (proposed) and black is HVFC (proposed).

4.1. Quantitative evaluation using the Weizmann database (Alpert et al., 2007)

In the quantitative part of the evaluation 23 test images (with ground truth data), having sharp edges with high curvature or weak contrast with unsettled edge-transition, have been chosen for a numerical evaluation process from the Weizmann dataset (Alpert et al., 2007) (see Fig. 3). For each algorithm, regions of interest are marked as an ellipse and initial contours are calculated as described in Section 3.3. We applied parameter settings for the compared methods according to the mentioned references to achieve the best performance. Like it was also mentioned in (Mishra et al., 2011), due to the intensity variation inside the object, this database is not suitable for ACWE method. Therefore, results were evaluated only for GVF, HGVF, VFC and HVFC algorithms.

For quantitative results we used the traditional *F*-measure score, which is the weighted, harmonic mean of precision and recall values:

$$F = \frac{2 \cdot \text{precision} \cdot \text{recall}}{\text{precision} + \text{recall}}. \tag{15}$$

According to the summarized results of 23 images, the average *F*-measure score (mean ± standard deviation) for each algorithm is the following:

GVF: 0.79 ± 0.09; HGVF: **0.87** ± **0.08**; VFC: 0.86 ± 0.07 and HVFC: **0.91** ± **0.06**. HGVF and HVFC provide higher *F*-measure score relative to the classical approaches.

Fig. 3 shows the detailed evaluation results for the 23 images separately. It is important to note that Harris based methods (HGVF and HVFC) outperform their traditional corresponding in nearly all of the cases.

4.2. Qualitative results for boundary accuracy

In the next part of the experiments, specific images were selected to show qualitative results (Figs. 4–6). The execution time of different methods for images **A**–**D** (with sizes 200×216, 300×200, 335×364 and 300×170) in Fig. 4 can be seen in Table 1. These experimental results were based on an Intel (R) Core (TM) i7 CPU with 4 GB RAM and MATLAB R2010b.

ACWE (Chan and Vese, 2001) method follows a level-set representation; therefore, it uses intensity homogeneity constraints instead of gradient based edge map. ACWE can successfully identify object boundaries even with high curvature parts, if intensity is homogeneous inside the object and the contour is closed properly (see image **A**, first row of Fig. 4). Else, ACWE converges to object parts representing homogeneous regions which differ largely from the estimated background (**B**–**D** images in Fig. 4).

Beside suffering from high curvature and low contrasted boundaries, as the detailed explanation showed in Section 2.2, GVF (Xu and Prince, 1997) also fails when the initial contour is further from the real boundary. In case of larger concavities of the object boundaries the convexity feature of the contour initialization step results in a distant initial contour, therefore, the method is trapped in local minima. The proposed HGVF improves the performance of the original method, by emphasizing low contrasted and high curvatures parts, therefore, it detects the peaks and the stem accurately in image **A**, and converges to the desired outline in image **D**. By enlarging a small part of image **D** having high curvature corners with weak edges, first and second row of Fig. 5 show the detailed detection result and the corresponding magnified force field of GVF and HGVF methods. Unlike the edge map of GVF, the proposed feature map of HGVF is able to lead the contour to the real boundary. However, when the concavity is larger (like in images **B** and **C**), HGVF still fails.

VFC (Li and Acton, 2007) has the advantage to be less sensitive to initialization than GVF, due to the calculated vector field kernel. Therefore, large concave outlines do not cause challenge (like image **B**), but the method fails to detect high curvature and low contrasted boundary parts due to the existing problems of the feature map (see Section 2.3 for further details).

The proposed HVFC method benefits from the advantages of traditional VFC algorithm and the introduced feature map of modified Harris function and detects the aforementioned complex boundaries accurately (see last column of Figs. 4 and 5).

Images **E**, **F** and **G** (with sizes 300×170, 300×170 and 282×191) in Fig. 4 show images containing Gaussian noise with different signal-to-noise ratio (SNR) and an originally blurred image to evaluate the robustness of the different methods against noise and blur.

For quantitative evaluation, **D**, **E** and **F** images were compared. The same parameter setting was applied in every case; therefore, we could test the robustness to noise. Image **D** was the original image without any additive noise, Image **E** with 5 dB SNR, Image **F** with 0.5 dB SNR. In Fig. 4, the results show that the proposed approaches are able to keep the main characteristics of the object outline, in Table 1(b) the corresponding quantitative *F*-measure scores can be seen.

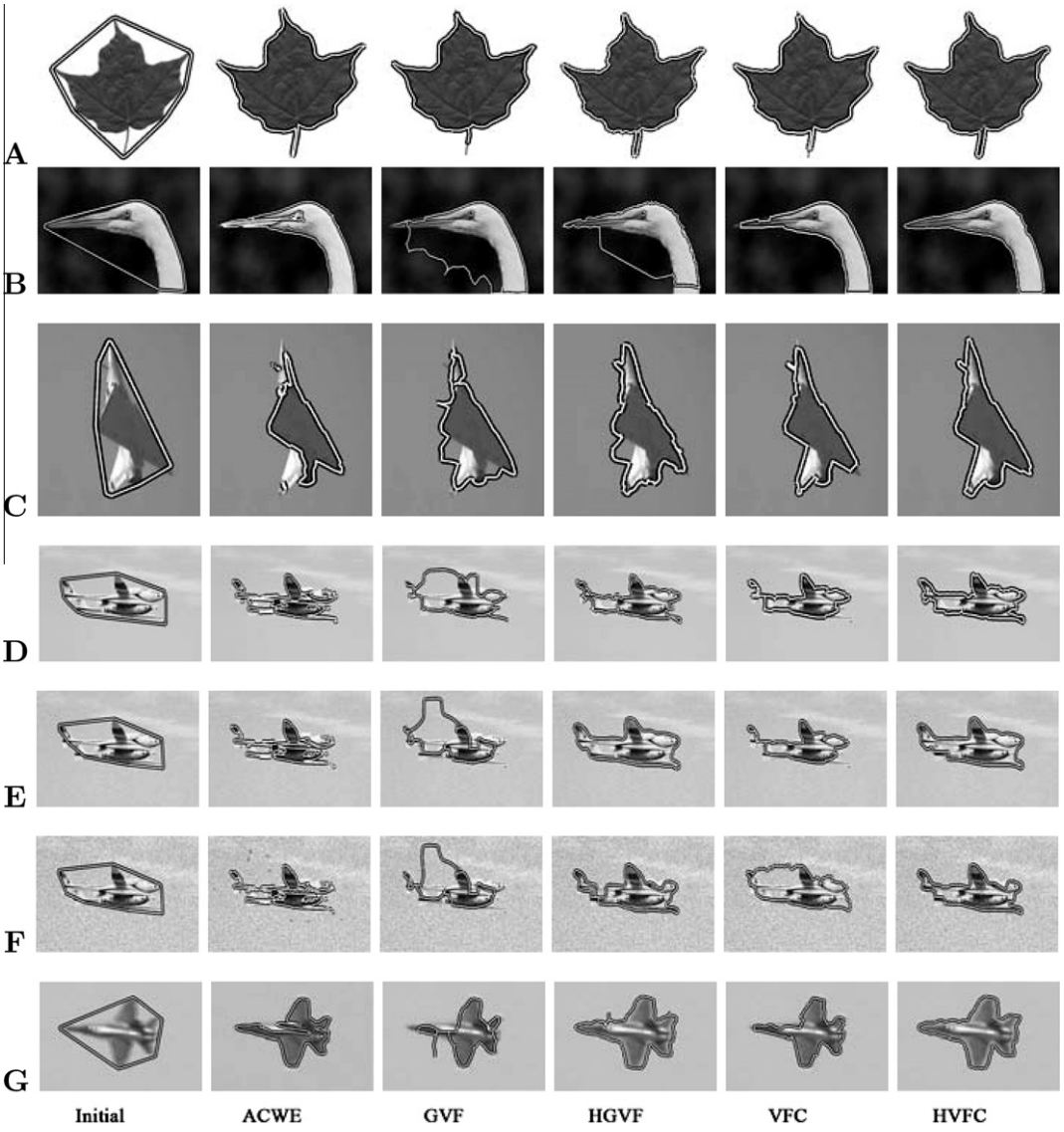

Fig. 4. Examples of contour detection: The first column shows the calculated initial contour (see Section 3.3). Second, third, fourth, fifth and sixth columns present the results for ACWE (Chan and Vese, 2001), GVF (Xu and Prince, 1997), HGVF (proposed), VFC (Li and Acton, 2007) and HVFC (proposed) methods.

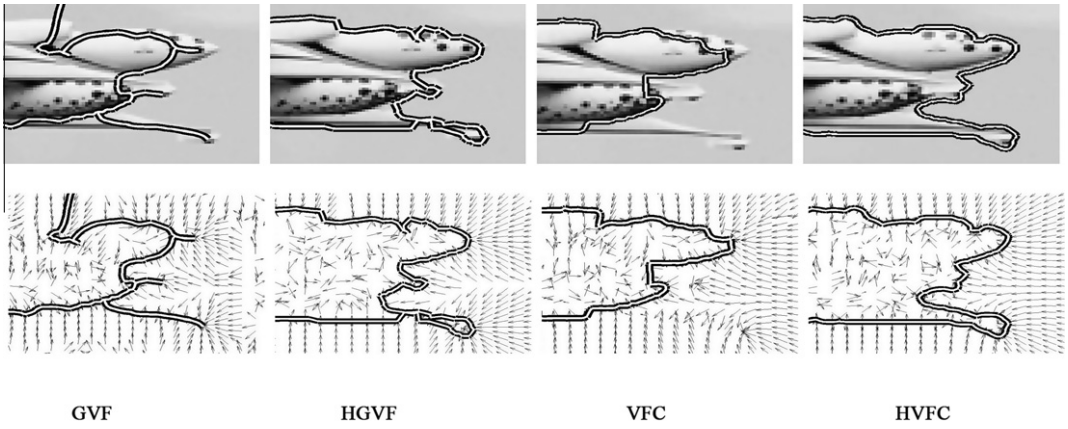

Fig. 5. Improvement of the different feature maps in image **D** achieved by modified Harris based characteristic function: the first row shows the image part with the detected outline, the second row is the corresponding force field and the contour. Columns show the results for GVF (Xu and Prince, 1997); HGVF (proposed); VFC (Li and Acton, 2007) and HVFC (proposed) methods.

In case of the blurred image **G**, HGVF and HVFC are able to converge to the real boundary more accurately than the compared GVF and VFC methods without skipping any object part with differing intensity as ACWE.

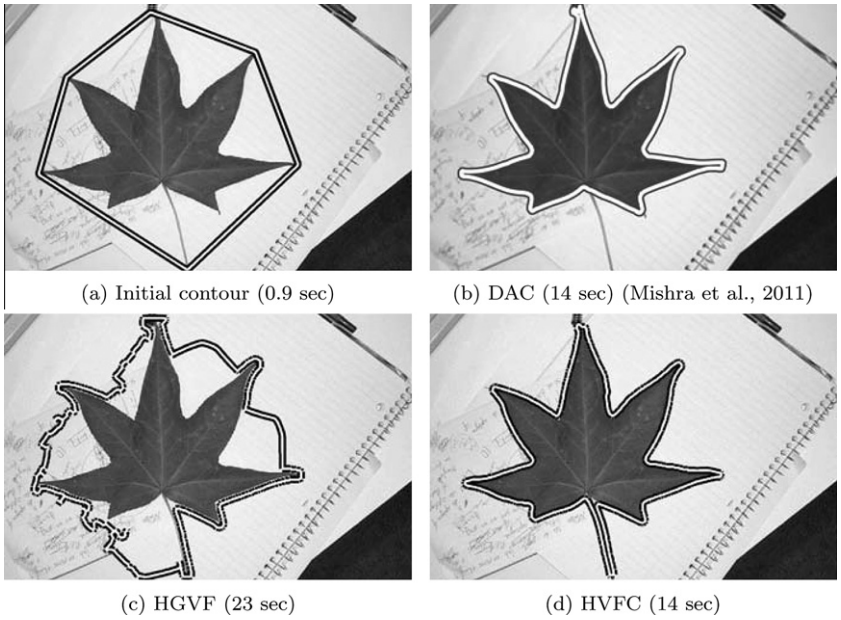

Fig. 6. Comparison with decoupled active contour (DAC) method (Mishra et al., 2011) with the execution time in brackets. (Image size: 450 × 297.)

Table 1
Performance of different active contour algorithms, including execution time for images without noise (a) and robustness to increasing Gaussian noise (b) for ACWE (Chan and Vese, 2001), GVF (Xu and Prince, 1997), HGVF (proposed), VFC (Li and Acton, 2007) and HVFC (proposed) methods.

(a) Execution times for images **A**–**D** in Fig. 4, IC indicates the initial contour

	Execution time [seconds]					
Images	IC	ACWE	GVF	HGVF	VFC	HVFC
A	0.36	13	5.8	5.6	3.7	4.8
B	0.44	66	6.2	6.7	4.2	5.1
C	0.85	68	9.4	11	6.3	6.9
D	0.38	12	3.9	4.3	3.2	3.7

(b) Robustness to noise for images **D**, **E** and **F** with increasing Gaussian noise, SNR indicates the signal-to-noise ratio, *F*-measure is given in Eq. (15)

	F-measure				
SNR	ACWE	GVF	HGVF	VFC	HVFC
∞ (image **D**)	0.66	0.64	0.89	0.79	0.93
5 dB (image **E**)	0.58	0.53	0.88	0.78	0.87
0.5 dB (image **F**)	0.60	0.52	0.86	0.74	0.87

Fig. 6 shows a comparison with the novel decoupled active contour method (Mishra et al., 2011) for an image with high curvature boundary parts. DAC addresses the limitations of traditional active contours (slow convergence rate and misconverging in the presence of noise or complex contours) by applying internal and external image forces independently. It consists of a measurement update step, employing a Hidden Markov model (HMM) and Viterbi search, and then a separate prior step, which modifies the updated curve based on the relative strengths of the measurement uncertainty and the non-stationary prior. We compared DAC with our proposed Harris based methods for image in Fig. 6, which was also used in (Mishra et al., 2011). Result of the comparison showed that DAC misses the stem and some peaks of the leaf. Although our proposed HGVF algorithm is not able to converge into large concavities (due to the aforementioned drawbacks), our HVFC approach detects the contour accurately. By considering the execution time of the different algorithms, HVFC is able to converge as fast as DAC.

5. Conclusion and future work

In this paper a novel feature map for GVF and VFC was introduced. This feature map is based on a modified Harris characteristic function, describes better the principal curvatures and emphasizes both corners and edges equally. Therefore, it can be used more efficiently for defining a new external force when detecting complex boundaries with weak contrast and high curvatures. An accurate initial contour is determined as the convex hull of the salient points of the feature map. Future work involves scale-space optimization (Lindeberg, 1996) of the smoothing scale and saliency radius around keypoints. Initial 3-D tests showed improvement in performance when extending the method to 3-D, compared with the traditional method. However, the three dimensional representation of Harris corner detector is quite novel (Glomb, 2009 and Sipiran and Bustos, 2011) and needs more extensive research and evaluation, which will be also included in the future work.

Acknowledgment

The authors thank the Reviewers as well as the Associate Editor, for their efforts to improve the paper. They would also like to thank for the published MATLAB code of the referenced active contour algorithms (Chan and Vese, 2001; Li and Acton, 2007 and Xu and Prince, 1997) used for comparison. This work was partially sup-

ported by the Hungarian Scientific Research Fund under Grant No. 76159.

References

Alpert, S., Galun, M., Basri, R., Brandt, A. 2007. Image segmentation by probabilistic bottom-up aggregation and cue integration. In: Proc. of IEEE Conf. on Computer Vision and Pattern Recognition, pp. 1–8.

Barber, C.B., Dobkin, D.P., Huhdanpaa, H., 1996. The quickhull algorithm for convex hulls. ACM Trans. Math. Softw. 22 (4), 469–483.

Bresson, X., Esedoglu, S., Vandergheynst, P., Thiran, J.-P., Osher, S., 2007. Fast global minimization of the active contour/snake model. J. Math. Imag. Vis. 28 (2), 151–167.

Brigger, P., Hoeg, J., Unser, M., 1997. B-spline snakes: A flexible tool for parametric contour detection. Internat. J. Comput. Vision 22 (1), 61–79.

Caselles, V., Kimmel, R., Sapiro, G., 1997. Geodesic active contours. Internat. J. Comput. Vision 22 (1), 61–79.

Chan, T.F., Vese, L.A., 2001. Active contours without edges. IEEE Trans. Image Process. 10 (2), 266–277.

Cheng, J., Foo, S., 2006. Dynamic directional gradient vector flow for snakes. IEEE Trans. Image Process. 15 (6), 1563–1571.

Chuang, C., Lie, W., 2004. A downstream algorithm based on extended gradient vector flow field for object segmentation. IEEE Trans. Image Process. 13 (10), 1379–1392.

Glomb, P. 2009. Detection of interest points on 3D data: Extending the Harris operator. In: 6th Internat. Conf. on Computer Recognition Systems, pp. 103–111.

Harris, C. Stephens, M. 1988. A combined corner and edge detector. In: Proc. of 4th Alvey Vision Conf., pp. 147–151.

Jifeng, N., Chengke, W., Shigang, L., Shuqin, Y., 2007. NGVF: An improved external force field for active contour model. Pattern Recognition Lett. 28 (1), 58–63.

Kass, M., Witkin, A.P., Terzopoulos, D., 1988. Snakes: Active contour models. Internat. J. Comput. Vision 1 (4), 321–331.

Kimmel, R., Bruckstein, A.M., 2003. Regularized Laplacian zero crossings as optimal edge integrators. Internat. J. Comput. Vision 53 (3), 225–243.

Kovacs, A., Sziranyi, T. 2010. High definition feature map for GVF snake by using Harris function. In: Proc. of Conf. on Advanced Concepts for Intelligent Vision Systems.

Kovacs, A. Sziranyi, T. 2011. Improved force field for vector field convolution method. In: Proc. of IEEE Internat. Conf. on Image Processing.

Kovacs, L., Sziranyi, T., 2007. Focus area extraction by blind deconvolution for defining regions of interest. IEEE Trans. Pattern Anal. Machine Intell. 29 (6), 1080–1085.

Li, B., Acton, T., 2007. Active contour external force using vector field convolution for image segmentation. IEEE Trans. Image Process. 16 (8), 2096–2106.

Lindeberg, T., 1996. Edge detection and ridge detection with automatic scale selection. Internat. J. Comput. Vision 30 (2), 465–470.

Mishra, A.K., Fieguth, P.W., Clausi, D.A., 2011. Decoupled active contour (DAC) for boundary detection. IEEE Trans. Pattern Anal. Machine Intell. 33 (2).

Schmid, C., Mohr, R., Bauckhage, C., 2000. Evaluation of interest point detectors. Internat. J. Comput. Vision 37 (2), 151–172.

Sirakov, Nikolay M., 2006. A new active convex hull model for image regions. J. Math. Imaging Vis. 26 (3), 309–325.

Sipiran, I., Bustos, B., 2011. Harris 3D: A robust extension of the Harris operator for interest point detection on 3D meshes. Visual Comput. 27 (11), 963–976.

Sundaramoorthi, G., Yezzi, A., 2007. Global regularizing flows with topology preservation for active contours and polygons. IEEE Trans. Image Process. 16 (3), 803–812.

Tauber, C., Batatia, H., Ayache, A., 2010. Quasi-automatic initialization for parametric active contours. Pattern Recognition Lett. 31, 83–90.

Uzunbas, M.G., Soldea, O., Unay, D., Cetin, M., Ünal, G.B., Erçil, A., Ekin, A., 2010. Coupled nonparametric shape and moment-based intershape pose priors for multiple basal Ganglia structure segmentation. IEEE Trans. Med. Imaging 29 (12), 1959–1978.

Vasilevskiy, A., Siddiqi, K., 2002. Flux maximizing geometric flows. IEEE Trans. Pattern Anal. Machine Intell. 24 (12), 1565–1578.

Wang, Y., Liu, L., Zhang, H., Cao, Z., Lu, S., 2010. Image segmentation using active contours with normally biased GVF external force. Signal Process. Lett. 17 (10), 875–878.

Xu, C., Prince, J. L. 1997. Gradient vector flow: A new external force for snakes. In: Proc. of IEEE Conf. on Computer Vision and Pattern Recognition, pp. 66–71.

Zamani, Fatemeh, Safabakhsh, Reza. 2006. An unsupervised GVF snake approach for white blood cell segmentation based on nucleus. In: Proc. of the 8th Internat. Conf. on Signal Processing.

Zhu, G., Zhang, S., Zeng, Q., Wang, C., 2010. Gradient vector flow active contours with prior directional information. Pattern Recognition Lett. 31, 845–856.